Available online at www.sciencedirect.com

ScienceDirect

Journal of Nuclear Materials 375 (2008) 80–85

journal of nuclear materials

www.elsevier.com/locate/jnucmat

# The influence of relative humidity on iron corrosion under proton irradiation

S. Lapuerta [a], N. Bérerd [a,b,*], N. Moncoffre [a], N. Millard-Pinard [a],
H. Jaffrézic [a], D. Crusset [c], D. Féron [d]

[a] *Institut de Physique Nucléaire de Lyon, Université de Lyon, Université Claude Bernard Lyon I, IN2P3/CNRS, 4 rue Enrico Fermi, 69622 Villeurbanne cedex, France*
[b] *Université de Lyon, Université Claude Bernard Lyon I, IUT A, département chimie, 94, boulevard Niels Bohr, 69622 Villeurbanne cedex, France*
[c] *ANDRA Parc de la Croix Blanche 1-7 rue Jean Monnet, F-92298 Châtenay-Malabry cedex, France*
[d] *Commissariat à l'Energie Atomique, CEA-Saclay, Service de la Corrosion et du Comportement des Matériaux dans leur Environnement, 91191 Gif-sur-Yvette cedex, France*

Received 26 January 2007; accepted 31 October 2007

## Abstract

With regard to the storage for high-level radioactive waste and the reversible period of a geological repository, the influence of proton irradiation on the indoor atmospheric corrosion of iron has been investigated in relation to the relative humidity (RH) in the atmosphere. Irradiation experiments were performed using a 3-MeV extracted proton beam. Relative humidity varies from 0% to 85%. Before and after each irradiation, the surfaces of the sample were characterised by Rutherford backscattering spectrometry in order to determine oxygen concentrations in the metal. The maximum oxidation rate was observed for 45% RH in air under proton irradiation and was compared with literature data without irradiation where the maximum oxidation rate was observed at 95% RH. The experimental results are discussed on the basis of the Langmuir–Hinshelwood (LH) model: they are explained by the contrast between the adsorption of $O_2$ and $H_2O$ species on the active cathodic sites of the iron surface and by the formation of $H^+(H_2O)_n$.

## 1. Introduction

Many concepts are developed for the management of high-level radioactive waste: several of them lead to an irradiation of the atmospheric corrosion of carbon steels. It is obvious for the storage of spend fuels packed in carbon–steel containers. In the French current concept for a long-term deep geological repository, stainless-steel containers of high-level nuclear waste will be protected by an overpack also made of carbon steel. During the first period, called the 'reversible period', which may extend over several decades or centuries, those overpacks will be exposed mainly to more or less humid air with an oxygen concentration that will decrease due to oxygen consumption by corrosion, for instance.

In a recent paper [1], the atmospheric corrosion mechanisms occurring within a rust layer during a wet–dry cycle were presented. Those results demonstrate the increase of iron corrosion by the joint effect of oxygen and water and the main influence of wet–dry cycles. In a previous work [2], we also showed that, under irradiation, a combination of oxygen and water molecules is needed to create a rust layer at room temperature. During storage and the first reversible period of the deep geological repository, there will be no wet–dry cycle. In order to understand

---

[*] Corresponding author. Address: Institut de Physique Nucléaire de Lyon, Université de Lyon, Université Claude Bernard Lyon I, IN2P3/CNRS, 4 rue Enrico Fermi, 69622 Villeurbanne cedex, France. Tel.: +33 4 72 43 10 57; fax: +33 4 72 44 80 04.

*E-mail addresses:* sandrine.lapuerta@cea.fr (S. Lapuerta), bererd@ipnl.in2p3.fr (N. Bérerd).

0022-3115/$ - see front matter © 2007 Elsevier B.V. All rights reserved.
doi:10.1016/j.jnucmat.2007.10.011

better the behaviour of carbon steel under those conditions and to go further in the interpretation of oxidation mechanisms, indoor atmospheric corrosion studies were performed on pure iron, with irradiation and relative humidity (RH) being the main parameters under study. The irradiation effect was investigated by using a 3-MeV proton beam characterised mainly by an electronic stopping power. Relative humidity varies between 0% and 85% for a given proton flux. The corrosion scale is characterised by using Rutherford backscattering spectrometry (RBS) and X-ray photoelectron spectroscopy (XPS). Experimental results are discussed on the basis of the Langmuir–Hinshelwood (LH) model.

## 2. Experiments

### 2.1. Irradiation conditions

Proton irradiations (3-MeV) are performed on the external beam line of the 4-MV Van de Graaff accelerator of the Nuclear Physics Institute of Lyon. The experimental set-up presented in Fig. 1 was described previously [2]. The beam is extracted from the vacuum by a 5-μm-thick Havar window and penetrates in the irradiation cell through the iron foil. Between the Havar window and the iron foil, protons go through an 8-mm wet-air gap. At that stage, the proton energy is 2.75 MeV and corresponds to a linear energy transfer in iron equal to 55.9 keV $\mu m^{-1}$. A sweeping system allows the homogeneous irradiation of a $5 \times 5$ $mm^2$ surface. A beam-current measurement is performed with a beam chopper placed in front of the Havar window. The beam intensity is set at 10 nA, which corresponds to a high irradiation flux of $2.5 \times 10^{11}$ p $s^{-1}$ $cm^{-2}$.

The iron foil is the sample on which atmospheric corrosion was investigated. Those samples consist of 10-μm-thick discs (25-mm diameter) made of pure iron (99.985% Fe).

RH is fixed according to the following set-up [2]: dry gas (20% $O_2$ + 80% $N_2$, or 100% $N_2$) is supplied from a bottle, whose flow is regulated by a manometer. The dry gas is saturated with water through a bubbling system and is adjusted to the proper RH value by using an alumina trap. That value is measured using a Hygropalm humidity controller. The system allows the RH to be set between 0% and 95%. In this paper, five RH values have been studied: 0%, 20%, 45%, 60% and 85%.

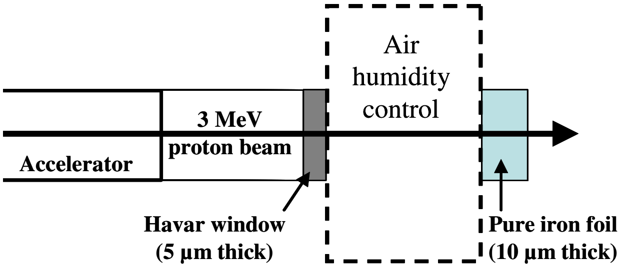

Fig. 1. Irradiation set-up.

### 2.2. Surface-characterisation techniques

One of the difficulties of those experiments was to quantify corrosion phenomena, since the testing period was quite short (less than 1 h) compared to standard testing conditions performed during atmospheric corrosion experiments that often last several days or even several years. Standard techniques like weight losses or thickness of the oxide layer determined by optical observations are not relevant. After investigation, RBS and XPS have been selected to characterise the corrosion scale. Before and after each irradiation, samples were analysed using RBS with 1.7–3-MeV alpha particles in order to determine oxygen-distribution profiles.

XPS experiments were also performed in order to characterise the near-surface chemical state of the corroded layer (iron and oxygen oxidation levels). Samples were first cleaned up with hexane, acetone and ethanol ultrasound baths to dissolve the superficial layer polluted mostly by carbon. In order to avoid any iron-oxide reduction, *in situ* surface ion-beam etching was never performed. Hence, only the very near-surface was analysed. High-resolution analyses were conducted on iron $2p_{3/2}$ and oxygen 1s signals. XPS measurements were performed with a SSI S-probe monochromatised spectrometer using Al-Kα X radiation. The analysed depth ranged from 3 to 5 nm and the analysed area corresponded to a $300 \times 1200$ μm spot.

## 3. Experimental results

Fig. 2 shows the RBS experimental spectra obtained for the non-irradiated sample and a corroded one irradiated during 45 min. From those spectra and using the SIMNRA software [3], oxygen concentration profiles were deduced. SIMNRA is used to reproduce experimental spectra by comparing simulated spectra. The latter are built according to a test-error procedure, assuming the elemental composition of the target.

The oxygen concentration distributions obtained for the 30 and 45-min irradiated samples are presented in Fig. 3

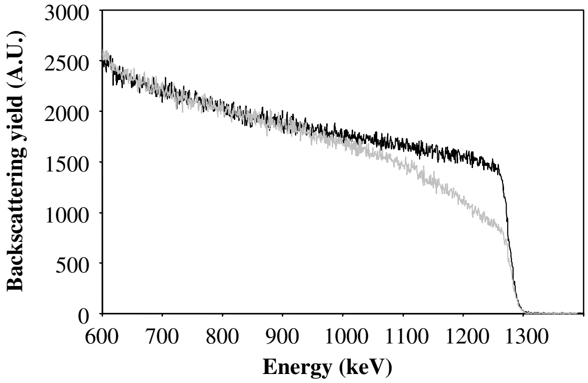

Fig. 2. Comparison of RBS experimental spectra corresponding to a non-irradiated sample (dark curve) and to a corroded one in humid air (light curve).

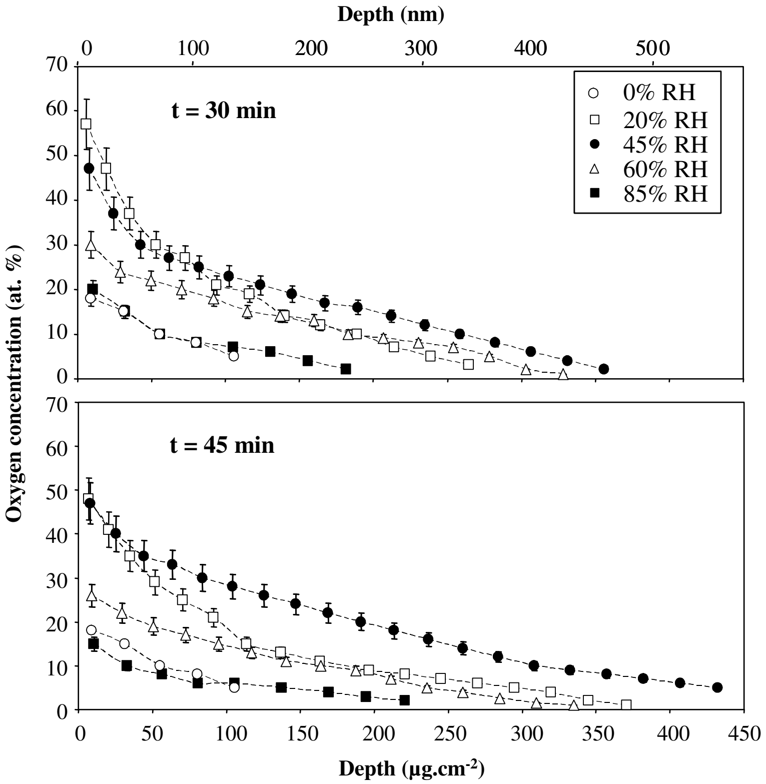

Fig. 3. Comparison of oxygen concentration profiles obtained after irradiation with different air relative humidities.

for RH values varying between 0% and 85%. These curves lead to several important and new observations, as follows:

- oxygen profiles are very low and similar with extreme RH values: 0% and 85%, which means that for both those RH values, the corrosion rate is nearly the same and very low. If that result was expected at 0% RH, it should be more surprising at 85% RH;
- those results show also that iron oxidation already occurs at a low RH (20%);
- that oxidation reaches a peak for an RH value close to 45%, and decreases at higher RH conditions.

The total amount of oxygen found in the oxide layer has been plotted in relation to relative humidity for an irradiation time of 45 min. The plot is displayed in Fig. 4 and shows that the variation goes through a maximum RH value roughly equal to 45% and that the quantity of resulting oxide is low and nearly the same at 0% and 85% RH under irradiation.

In order to identify the surface-oxidation states of iron and oxygen, XPS analyses have been performed on irradiated samples at 45% and 85% RH. The obtained data from a non-irradiated sample are also presented for reference purposes and called ‘blank’. XPS spectra are displayed in Fig. 5. On the basis of literature data [4], the binding-energy positions of the different Fe $2p_{3/2}$ and O 1s contributions have been pointed out in the figure. The iron signal shows that irradiated samples at 45% and 85% RH correspond to 100% $Fe^{3+}$, whereas the oxygen peaks are different between both samples. It should be noticed also that carbon pollution is observed in all samples, as already mentioned in many XPS studies.

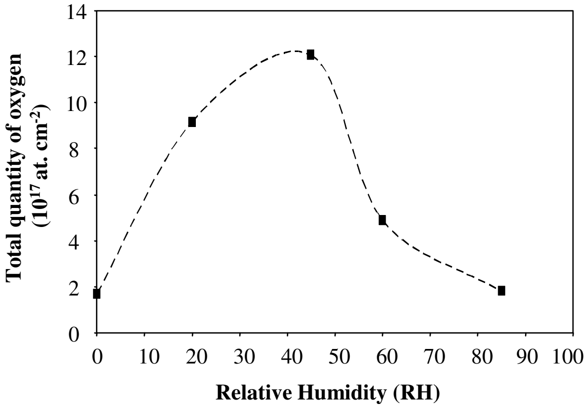

Fig. 4. Oxygen gain as function of RH for 45 min irradiated samples.

From the oxygen-peak decomposition, the relative percentages of oxide and hydroxide contributions at the surface have been determined [5,6], as well as the water content (absorbed water molecules). They are summarised in Table 1.

Table 1 shows that the oxide layer is a mixture of iron-oxide and hydroxide phases at 45% and 85% RH and that the adsorbed water quantity at 85% RH is three times greater than that obtained at 45%.

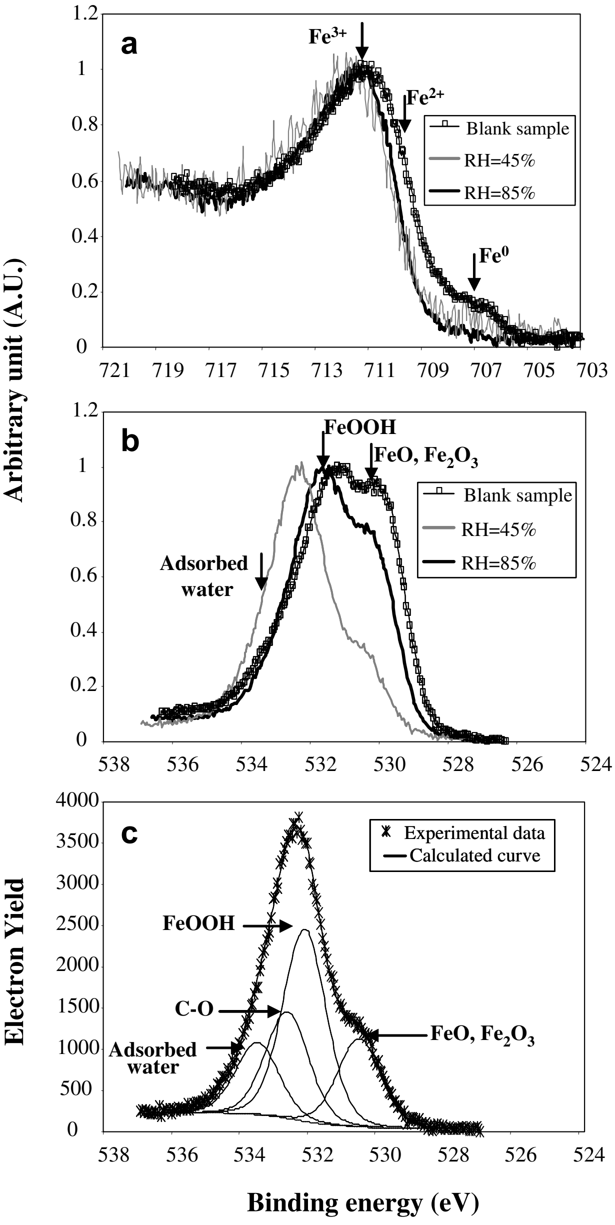

Fig. 5. (a) Iron $2p_{3/2}$ and (b) oxygen 1s XPS signals obtained on the samples irradiated at 45% RH and 85% RH. Oxygen 1s peak decomposition for a 30 min irradiated sample at 85% RH (c).

Table 1
Relative percentages of the compounds identified by XPS at the near sample surface

| | $Fe_2O_3$, FeO | FeOOH | C–O | Adsorbed water |
|---|---|---|---|---|
| Blank sample | 41 | 38 | 15 | 6 |
| Irradiated sample at 45% RH | 37 | 41 | 17 | 5 |
| Irradiated sample at 85% RH | 19 | 42 | 23 | 16 |

## 4. Discussion

Atmospheric corrosion is an aqueous-corrosion phenomenon with anodic and cathodic reactions occurring in the condensed water layer when RH is lower than 100%, or in the aqueous phase during wet cycles [7]. Under the experimental conditions of this study, two main cathodic reactions (1), (2) may be considered:

$$1/2O_2 + H_2O + 2e^- \rightarrow 2OH^-, \tag{1}$$

$$H^+(H_2O)_n + e^- \rightarrow 1/2H_2 + n(H_2O), \tag{2}$$

Cathodic reaction (1) is always involved in atmospheric corrosion, while cathodic reaction (2) is specific to irradiation conditions and relates to the production of clusters like $H^+(H_2O)_n$ during the radiolysis of humid air [8]. It must be emphasised that reaction (2) releases water molecules at the surface of the sample.

Anodic reactions are more often assumed to be:

$$Fe \rightarrow Fe^{3+} + 3e^-. \tag{3}$$

$$\text{or/and } Fe \rightarrow Fe^{2+} + 2e^-. \tag{4}$$

In a previous paper [2], we have studied the influence of gas composition ($N_2 + H_2O$, $N_2 + O_2$, $N_2 + O_2 + H_2O$) on the corrosion of pure iron under proton irradiation. In the experimental conditions of the study, it was clearly demonstrated that the coupling of $O_2 + H_2O$ species was a necessary condition to oxidise iron. No oxidation was observed without oxygen or without vapour. Oxygen and vapour ($O_2$ and $H_2O$) were required to obtain an oxide layer under irradiation. Hence, only Eqs. (1), (3), and (4) may be considered, in a first approximation, leading to the formation of FeO, FeOOH and $Fe_2O_3$.

In order to explain our results displayed in Fig. 4, we assume that $O_2$ and $H_2O$ molecules are adsorbed on the same active site ($S_{surface}$) of the iron surface. We also assume that reaction (1) governs the overall reaction kinetics. That leads to consider the LH model for bimolecular reactions, described by the following equations:

$$O_2 + S_{surface} \leftrightarrow O_2\text{–}S_{surface}, \tag{5}$$

$$H_2O + S_{surface} \leftrightarrow H_2O\text{–}S_{surface}. \tag{6}$$

The adsorption rate of $O_2$ and $H_2O$ may be written as follows:

$$\frac{d\theta_{O_2}}{dt} = k_a(1 - \theta_{O_2} - \theta_{H_2O})P_{O_2} - k_d\theta_{O_2}, \tag{7}$$

$$\frac{d\theta_{H_2O}}{dt} = k'_a(1 - \theta_{H_2O} - \theta_{O_2})P_{H_2O} - k'_d\theta_{H_2O}, \tag{8}$$

where $\theta_{O_2}$ and $\theta_{H_2O}$ are the $O_2$ and $H_2O$ fractional coverages, respectively, which are directly related to partial pressures $p_{O_2}$ and $p_{H_2O}$; $k_a$ and $k_d$ are the oxygen-adsorption and desorption rate constants, respectively, whereas $k'_a$ and $k'_d$ are the water-adsorption and desorption rate constants.At steady state:

$$\theta_{O_2} = K_{O_2}p_{O_2}\theta_s, \tag{9}$$

$$\text{and } \theta_{H_2O} = K_{H_2O}p_{H_2O}\theta_s, \tag{10}$$

with $K_{O_2} = \frac{k_a}{k_d}$, $K_{H_2O} = \frac{k'_a}{k'_d}$ and $\theta_s = 1 - (\theta_{O_2} + \theta_{H_2O})$.

Since the corrosion rate, *R,* is equal to:

$$R = k \cdot \theta_{O_2} \cdot \theta_{H_2O}, \tag{11}$$

where $k$ is a kinetic constant, hence

$$R = k \cdot \frac{K_{O_2} \cdot p_{O_2} \cdot K_{H_2O} \cdot p_{H_2O}}{(1 + K_{O_2} \cdot p_{O_2} + K_{H_2O} \cdot p_{H_2O})^2}. \tag{12}$$

Under our experimental conditions, the partial pressure of oxygen is constant. Consequently, the $k_{H_2O} \cdot p_{H_2O}$ product, relating to the RH value, is the only variable.

From Eq. (11), it turns out that for high coverages of either $H_2O$ ($\theta_{O_2} = 0$) or $O_2$ ($\theta_{H_2O} = 0$), the corrosion rate becomes equal to 0. In addition, Eq. (12) shows that the corrosion rate, *R,* goes through a peak.

That interpretation is consistent with our experimental results. Indeed, as displayed in Fig. 4 and Table 1, iron oxidation is very weak at 0% and 85% RH values. For an RH equal to 85%, the amount of adsorbed water is close to a peak, whereas in dry air (RH = 0), oxygen-adsorption is close to its peak. In both cases, nearly no oxidation was observed.

In order to discuss the irradiation effect on iron corrosion, we have compared the results we obtained under irradiation together with atmospheric corrosion results from the literature [1,9]. That comparison is summarised in Table 2. Without irradiation, the corrosion rate becomes significant for RH values higher than 60% and the process reaches a peak for high RH (often greater than 95%). Those observations are explained by the formation of a water layer that starts to form at an RH value close to 60% (40% for some authors, depending on the properties, roughness, pollutants of the surface, etc.). The water layer catalyses oxygen reduction on iron as expressed by Eq. (1) and initiates iron corrosion. In comparison, the peak of the corrosion rate under irradiation is reached at lower RH values (45%).

Those differences between the results obtained with and without irradiation are explained by the fact that a water layer (several atomic monolayers) is needed on the iron surface in order to catalyse the cathodic reaction. It is the reason with dry air is not corrosive for iron, even if oxygen is the oxidant of atmospheric corrosion phenomena. Under irradiation, not only oxygen, but also other oxidants such as $H_2O_2$, $O_2^{\cdot}$, etc., which may be produced by radiolysis, will be involved in the cathodic reaction, only if they are dissolved in a water layer on the iron surface. They occupy probably the same active sites as oxygen and water.

On the other hand, under irradiation, the formation of $H^+(H_2O)_n$ clusters is induced by wet air radiolysis [8]. The migration of the electrical charges carried on by protons under irradiation induces an electrical field in the sample, which has the same direction as the beam. In a previous paper [10], we have used the point-defect model [11] in order to estimate the electrical field, *E,* at 168 V $cm^{-1}$. We may assume that the electrical-field gradient increases the adsorption rate of those clusters. It also enhances their dissociation in $nH_2O$ and $H^+$ species, the $H^+(H_2O)_n$ clusters being attracted to the surface of the sample. Hence, the fractional coverage of the water is more important under irradiation than without at a similar RH and that may explain why differences were observed between our experimental results and those obtained under atmospheric corrosion. The explanation regarding the effect of clusters is consistent with the decrease in the corrosion rate observed at high RH under irradiation (Fig. 4) and with the minor role played by oxidising species produced by water radiolysis, even if they probably enhance corrosion phenomena when a water layer is present on the iron surface.

Table 2
Irradiation effect on iron corrosion

| | Under irradiation (%) | Without irradiation [1,9] (%) |
|---|---|---|
| RH required for corrosion initiation | <20 | 60 |
| RH of maximum of corrosion rate | 45 | 95 |

## 5. Conclusion

The evolution of the oxidation curve (Fig. 4), which shows nearly no atmospheric corrosion of iron under irradiation at 0% and 85% RH, has been explained using the LH model: the formation of $H^+(H_2O)_n$ clusters contributes to the saturation of adsorption sites at the surface of the sample by water molecules and explains the low corrosion at high RH. Moreover, under irradiation, the RH influence on the corrosion rate has been shown to be different from the one without irradiation: maximum corrosion is observed at 45% RH under irradiation while, that peak is generally observed at RH values of 95% or higher when there is no irradiation. Under irradiation, the beginning and the peak of the corrosion process are observed for low RH values (i.e., where nearly no atmospheric corrosion is observed without irradiation): once again, that phenomenon is explained by $H^+(H_2O)_n$ clusters that contribute to the formation of a water layer on iron and to the cathodic reaction (2), even if probably oxidant species, such as $O_2$, $H_2O_2$, etc., are also involved in cathodic reactions and increase corrosion phenomena, but only when the water layer is formed on the iron surface.

Those results do not represent only an important step in forecasting the atmospheric corrosion behaviour of iron overpacks for radioactive waste-disposal purposes, they also have to be applied to the understanding of atmospheric corrosion phenomena under and without irradiation:

- those results confirm the major influence of the water layer in atmospheric corrosion;
- the importance of adsorption sites is not addressed very often, but has been shown to play a major role, at least at the beginning of atmospheric corrosion.

## Acknowledgement

The authors would like to thank Mrs Noëlle Chevarier for her most helpful contribution through fruitful discussions.

## References

[1] S. Hoerlé, F. Mazaudier, Ph. Dillmann, G. Santarini, Corr. Sci. 46 (2004) 1431.

[2] S. Lapuerta, N. Moncoffre, N. Bérerd, H. Jaffrezic, N. Millard-Pinard, D. Crusset, Nucl. Insturm. Meth.B 249 (2006) 470.

[3] M. Mayer, SIMNRA User's Guide, Report IPP 9/113, Max-Planck-Institut für Plasmaphysik, Garching, Germany, 1997.

[4] T.-C. Lin, G. Seshadri, J.A. Kelber, Appl. Surf. Sci. 119 (1997) 83.

[5] I.D. Welsh, P.M.A. Sherwood, Phys. Rev. B 40 (1989) 6386.

[6] S. Suzuki, K. Yanagihara, K. Hirokawa, Surf. Interface Anal. 30 (2000) 372.

[7] P. Marcus, Corrosion Mechanisms in Theory and Practice, second Ed., Marcel Dekker Inc, 1995.

[8] L. Wayne-Sieck, T.J. Buckley, J.T. Herron, D.S. Green, Plasma Chem. Plasma Process. 21 (2001) 441.

[9] T.E. Greadel, R.P. Frankenthal, J. Electrochem. Soc. 137 (1990) 2385.

[10] S. Lapuerta, N. Moncoffre, H. Jaffrezic, N. Millard-Pinard, N. Bérerd, C. Esnouf, D. Crusset, J. Appl. Phys. 101 (2007), doi:10.1063/1.2711759.

[11] C.Y. Chao, L.F. Lin, D.D. Macdonald, J. Electrochem. Soc. 128 (1981) 1187.